Iraqi Journal for Applied Science (IJAS)
Vol. 3, No. 2, June, 2026, pp. 69-76
E-ISSN: 3006-5828 DOI: 10.69923/2nrc6545

Research Article

Adsorption of chromium ions using two types of aqueous biochar

Safa A. Yassin
The General Directorate for Education of Diyala. Diyala Governorate, Iraq.

Article Information

Article history:

Received: 10, 01, 2025
Revised: 30, 04, 2026
Accepted: 12, 05, 2026
Published: 30, 06, 2026

Keywords:

Biochar
Adsorption
Chromium ions Cr(VI)

Abstract

Biochar is a porous, carbon-rich substance created when biomass is thermally broken down in an oxygen-limited environment. The removal of chromium ions from polluted water has been extensively investigated because of its large surface area and surface functional groups. This study observes the production of biochar from a variety of biomass sources, such as *Pomegranate husks* (Po-Biochar) and animal *waste* (An-Biochar), and assesses how well these methods remove Cr(VI) from aqueous solutions. FTIR, FE-SEM, and BET were used to describe the biochar samples. The effects of pH, contact duration, Cr(VI) concentration, and biochar dose were evaluated using adsorption studies. According to the data, An-Biochar exhibited the maximum adsorption capacity. The adsorption process also followed pseudo-second-order kinetics, and the Freundlich isotherm was found to be the best one that can describe the adsorption of chromium ions Cr(VI) over Po-Biochar and An-Biochar samples, compared with the Langmuir isotherm, all of which were noted from the correlation coefficients values R^2.

Corresponding Author: ***Corresponding Author:*** *Safa A.Yassin, General Directorate for Education of Diyala.*
E-mail *:safaahmed072@gmail.com*

1. INTRODUCTION

The primary sources of chromium (Cr (VI)) contaminants in the environment are wastewater and industrial effluents. Cr (VI) contamination has emerged as one of the most significant environmental issues worldwide because of its lengthy environmental persistence and extremely lethal nature to living things [1]. Cr (VI) is one of the most prevalent environmental pollutants and is extremely harmful due to its extensive industrial use. Because Cr (VI) is often non-biodegradable, it pollutes the soil and water, remains in the environment for a long time, and poses serious health hazards to both people and wildlife. The hexavalent form of Cr is mutagenic, genotoxic, and carcinogenic. The present physicochemical methods for removing Cr (VI) are not eco-friendly and require a large number of chemicals [2,3]. Chromium poses significant threats to ecosystems and human health because of its high mobility and bioaccumulation capacity. Biochar, produced via biomass pyrolysis, has emerged as a promising low-cost adsorbent for heavy metal removal [4].

The physicochemical characteristics of the end product, the pyrolysis conditions, and the type of biomass feedstock affect its adsorption effectiveness [5,6]. The intended usage and ultimate effects of biochar's can be directly controlled by their structural and physicochemical characteristics [7]. Heavy metal pollution such as that caused by Cd, Hg, Pb, Cu, Ni, Zn, As, and Cr—has become a major problem worldwide. Adsorption processes are one of the most well-known remediation techniques due to their affordability, ease of use, and environmental sustainability. Biochar has attracted a lot of attention in this area because of its intriguing adsorption capabilities [8,9]. The neurological system, some organs with detoxifying roles, and the functioning of enzymes can all be seriously harmed by prolonged exposure to heavy metal ions. Therefore, drinking water tainted with heavy metals can directly harm human health [10,11]. This study examines the synthesis of biochar from various sources, along with its potential for eliminating Cr(VI) ions from aquatic environments.

2. METHOD

We purchased sodium dichromate dihydrate ($Na_2Cr_2O_7•2H_2O$) from Sigma Aldrich. Animal manure and pomegranate husks were acquired from an Iraqi farm. An FTIR-type SHIMADZU spectrometer from Japan was used to record FTIR spectra. A BET Quantachrome Nova1000e (Germany) was used to quantify the surface area. Biochar was produced using a BINDER oven (Hotline International, 20-360, Germany). A pH meter on the Sigma -BP3001 (Germany) was used to measure the acidity of the product, and a field emission-scanning electron microscopy (FE-SEM) on the ZEISS model: Sigma VP was used to assess the morphology of the product.

a. Biomass Feedstocks

Pomegranate husks and animal waste were the two-biomass types chosen as the raw materials for biochar manufacturing, Figure 1.

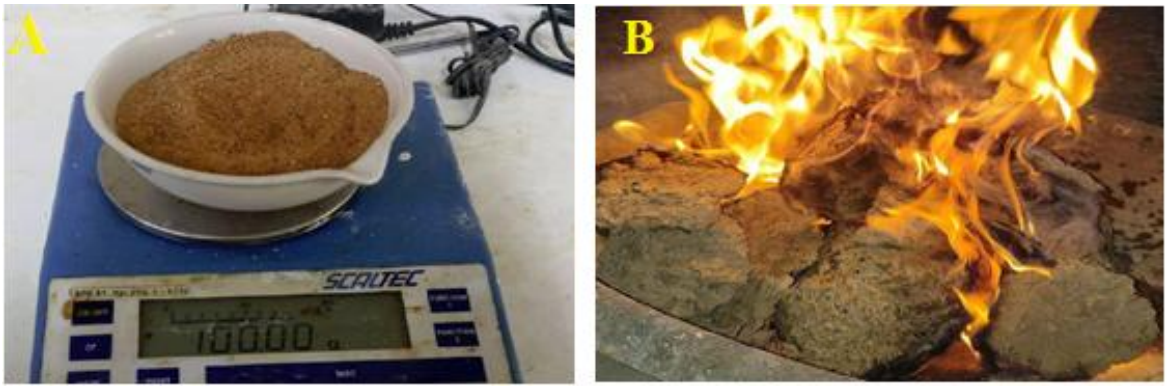

Figure 1. Biomass feedstocks of (A) Pomegranate husks (Po-biochar) and (B) animal waste (An-biochar)

b. Biochar Production

Slow pyrolysis was used to create the biochar in a furnace at 700°C for 5 h with little oxygen. After being crushed and sieved to a particle size of less than 1 mm, the resultant biochar was stored in airtight containers for later use, Figure 2.

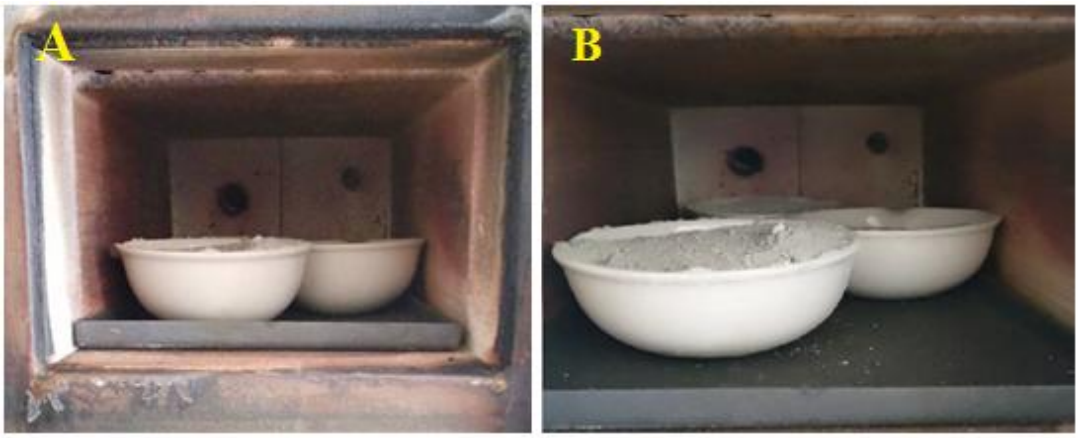

Figure 2. Biochar production of (A) Pomegranate husks (Po-biochar) and (B) animal waste (An-biochar)

The following acronyms were used to identify the various forms of biochar: Pomegranate husks (Po-biochar) and animal waste (An-biochar).

c. pH Measurements

The pH of the leachate produced in the manner outlined below has been tested. Before the measurement, biochar was placed in a 100 mL test tube, well mixed with deionized water (DIW) at a 1:20 ratio (0.5 g biochar:10 ml DIW), shaken for 30 min at 40°C, and left to stand for 40 min. A pH meter (Mettler Toledo, USA) was used to measure the pH.

d. BET (Brunauer-Emmett-Teller) Surface Area

The Brunauer-Emmett-Teller (BET) technique was used to determine the surface area, average pore volume, and average pore diameter of the prepared biochar, while nitrogen (N_2) was adsorbed at 77 K. The TriStar II Plus analyzer (Micromeritics, USA) was used to perform the analysis in the Tehran University/College of Science. The nitrogen gas adsorption and desorption volumes at various relative pressures serve as the foundation for this technique.

e. Biomass Pyrolysis

For 5 h, biochar was pyrolyzed in a furnace with a regulated heating rate of 20°C per minute and a restricted oxygen atmosphere at 700°C. Each biochar was made from ~100 g of biomass, and the yield was determined using Equation [1,12].

$$Biochar\ yield\ (\%) = \frac{Wf}{Wi} x100 \qquad (1)$$

Where W_f = mass (g) after pyrolysis and W_i = mass (g) before pyrolysis.

3. RESULTS AND DISCUSSION

3.1. To identify functional groups on the biochar surface, Fourier transform IR spectroscopy (FTIR).

Figure 3 shows the FTIR spectra of biochar's made from pomegranate husks (Po-Biochar) and animal manure (An-Biochar) at a pyrolysis temperature of 700 °C are displayed in Figure 3. As anticipated, notable alterations were observed in the chemical and structural contents of biochar when different biochar sources were used. The FTIR approach might be used to properly track these changes. Band allocations for biochar's have been thoroughly examined from various sources [13]. Several characteristic bands, such as those at 3452 cm^{-1} and 3425 cm^{-1} (O-H stretching vibrations of hydrogen bonded hydroxyl groups), 2997 cm^{-1} and 2970 cm^{-1} (asymmetric and symmetric C-H stretching vibrations for aliphatic groups), 1797 cm^{-1} (carboxyl C=O stretching mode), and 1053 cm-1 (symmetric C-O stretching), decreased when using different biochar sources in addition to the previously noted results. Several bands have become more intense in this biochar source, such as the aromatic C-H deformation modes at 875 cm^{-1} and 713 cm^{-1}, the aromatic C=C and C=O stretching modes of conjugated ketones and quinones at 1431 cm^{-1} and 1458 cm^{-1}, and the aromatic C-C stretching vibrations in the aromatic ring at 1408 cm^{-1} and 1403 cm^{-1}.

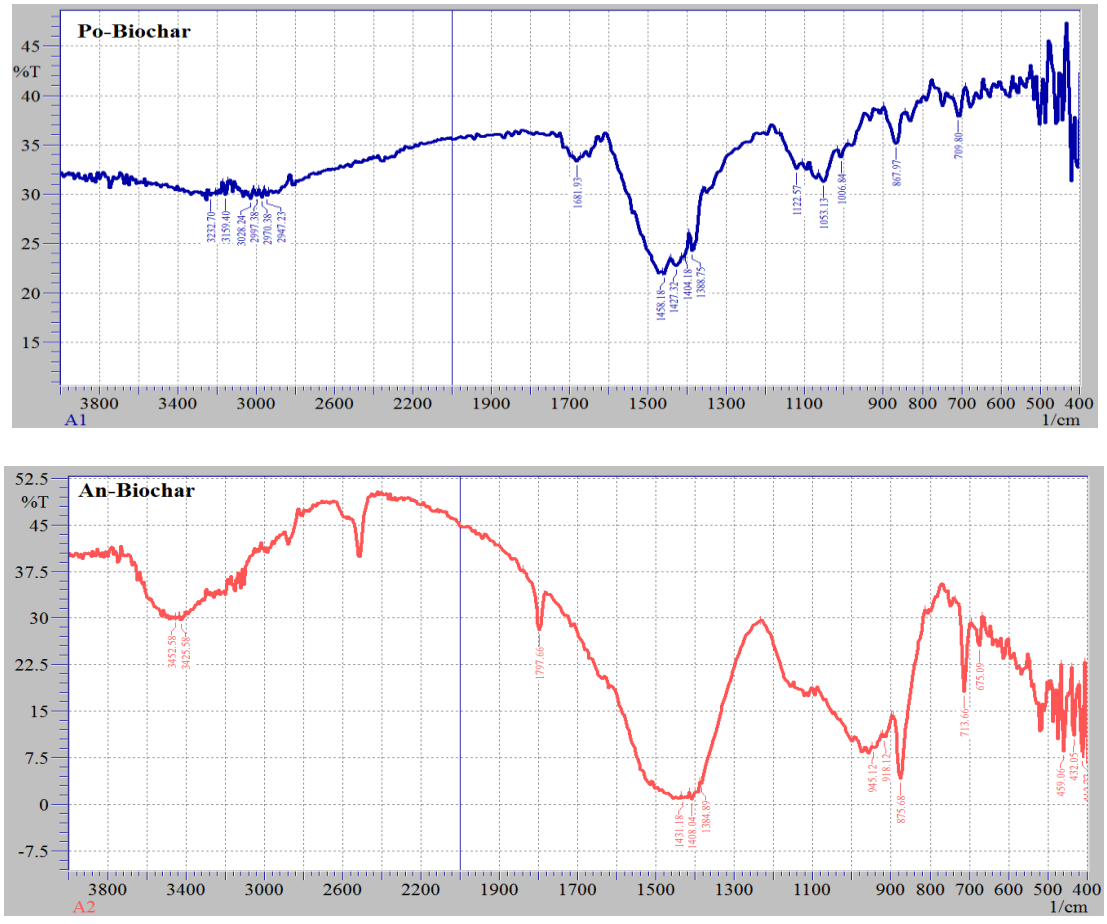

Figure 3. FTIR spectra of Po-biochar and An-biochar

The surface morphology and porosity of the produced biochar were determined using field emission-scanning electron microscope (FE-SEM) techniques. The FE-SEM images of the two biochar materials. Po-Biochar and An-Biochar, are displayed in Figures 4 (a) and (b). The biochar materials flake-like shape and size variation in the micrometer range are evident from the Po-Biochar FE–SEM image. The Po-Biochar sample did not show any hollow structures because the pomegranate husks were sintered at 700 °C and became more amorphous in nature. Figure 4 (b) shows the FE-SEM image of An-Biochar, which clearly shows the hollow structures which are in µm sizes.

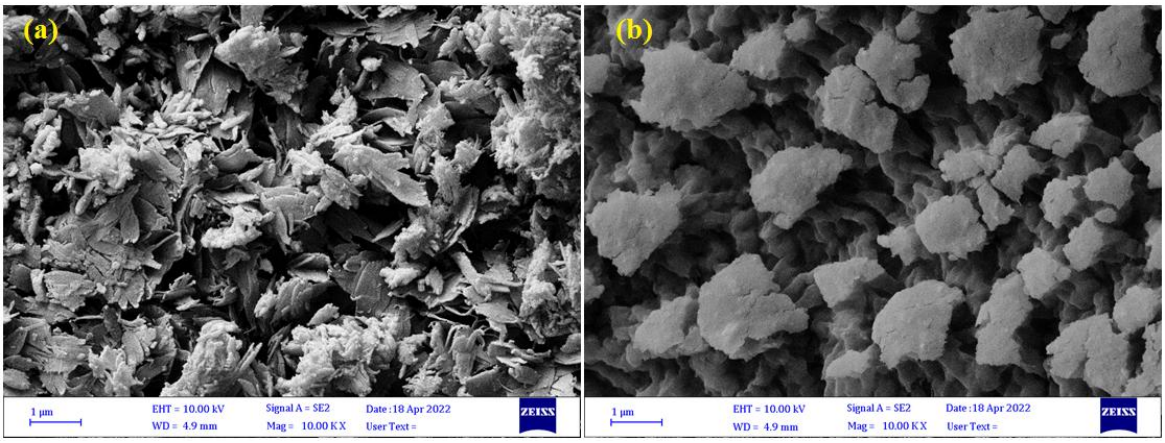

Figure 4. FE-SEM images of (a) Pomegranate husks (Po-Biochar) and (b) animal waste (An-Biochar).

3.2. The Brunauer–Emmett–Teller (BET)

BET analysis was used to determine the surface area and pore volume. Figure 5 (a and b) displays the BET specific surface area isotherms of the modified biochar materials (Po-Biochar and An-Biochar). The isotherm was attributed to the type IV form and the H_2-type hysteresis loop. The specific surface areas of Po- and An-biochar's were 49.58 and 63.81 $m^2\ g^{-1}$, respectively. Figures 5(c) and (d) show the pore distribution curve obtained using the Barrett–Joyner–Halenda (BJH) approach. Po-Biochar and An-Biochar have pore diameters of 17.52 and 26.38 nm, respectively. According to the results, the produced An-Biochar materials have a mesoporous surface with a high specific surface area. Furthermore, based on the adsorption isotherm data, the total pore volume was estimated to be approximately 0.54 $cm^3\ g^{-1}$ for Po-biochar and 0.53 $cm^3\ g^{-1}$ for An-biochar, indicating very similar pore volumes for both materials. The pore size distribution curves reveal that Po-biochar exhibits a broader distribution ranging from approximately 10 to 80 nm with a dominant peak around 20–25 nm, while An-biochar shows a relatively narrower distribution between 10 and 60 nm with a main peak around 18–22 nm. These findings confirm that both materials possess a mesoporous structure, with Po-biochar having a wider pore distribution and An-biochar exhibiting a more uniform pore structure, which may contribute to the differences in adsorption behavior.

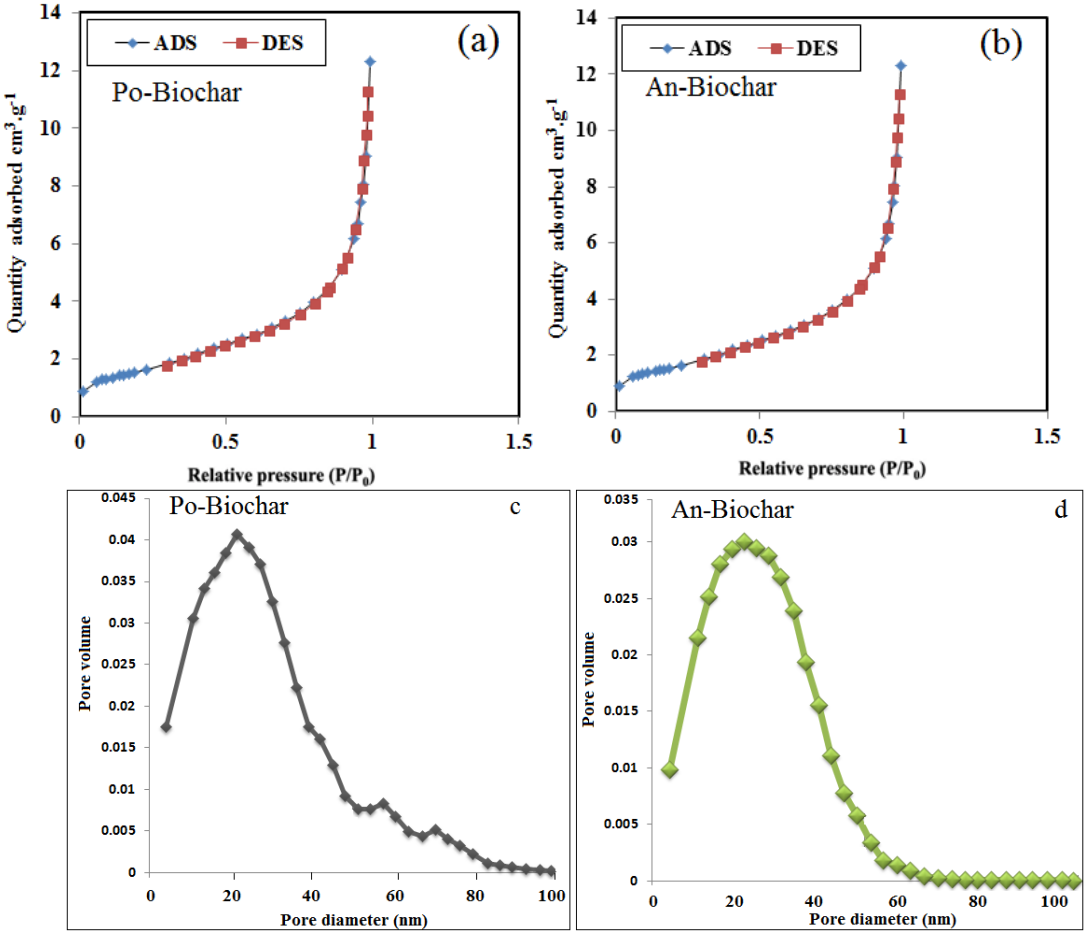

Figure 5. Nitrogen adsorption–desorption isotherms of (a) Po-biochar and (b) An-biochar. BJH adsorption pore size distribution curves of (c) Po-biochar and (d) An-biochar.

3.3. Adsorption studies

3.3.1 Comparison of An- and Po-Biochars

Figure 6 (a - c) shows the comparison findings for the adsorption of Cr(VI) chromium ions for both Po- and An-biochar. Figure 6(a - c) shows that the An- Biochar sample effectively absorbed chromium. This variation in the sorption capacity of chromium ions Cr(VI) on various biochar's might be caused by a number of factors, including variations in the molecular weight and chemical structure of each species. In contrast to the Po- Biochar materials figure 6(a - c) , the An-biochar materials effectively adsorbed the Cr(VI) ions. The difference between the initial (Ci) and equilibrium (Ce) concentrations of liquid Cr(VI) following filtration was used to calculate the removal efficiency of Cr(VI) onto the produced Po- and An-biochar. The following formulas were used to determine the adsorption capacity and chromium ion Cr(VI) removal efficiency of biochar [14]:

$$Removal\ (\%) = \frac{Ci-Ce}{Ci} \text{ x } 100 \qquad (2)$$

$$qe\ = \frac{(Ci-Ce)v}{W} \qquad (3)$$

where W is the weight of the adsorbent in grams (g), v is the volume of the Cr(VI) ion solution (L), and Ci and Ce are the initial and equilibrium concentrations of Cr(VI) chromium ions, respectively; Ce is the concentration of Cr(VI) chromium ions, and qe is the equilibrium adsorption capacity.

3.3.1. Effect of the contact time

The effect of contact time on the efficiency of the removal of Cr (VI) ions by Po-Biochar and An-Biochar was investigated at different time intervals up to 300 min. Figure 6 (a) demonstrates that the adsorption of Cr(VI) ions rose quickly within the first 20 min, and the removal efficiency approached 50%. Subsequently, the adsorption rate steadily dropped until equilibrium was reached, which took approximately 160 min, with maximum removal efficiencies of 91% and 86% for An- and Po-biochar, respectively. The equilibrium period of both adsorbates was 160 min; however, An-Biochar had a distinct Cr(VI) ion adsorption pattern in contrast to Po-Biochar. Within 20 min, 20% of the **Cr(VI)** ions were quickly eliminated, as shown in Figure 6(a). Subsequently, the adsorption rate decreased until it reached equilibrium at a maximum removal effectiveness of 91%, which took approximately 160 min. The comparatively quick adsorption of **Cr(VI)** ions onto the An-Biochar materials was most likely caused by the high attraction of the pollutants to a large number of binding sites that originated from the surface of the materials. Because the accessible binding sites on the An-Biochar surface were occupied, the adsorption was slower than in the early stages. The findings indicated that the equilibrium time for both pollutants was approximately 160 min.

3.3.2. Effect of the pH

Considering other factors during the adsorption process, the initial pH of the aqueous medium is particularly important because the characteristics of both the adsorbent and the adsorbate can be affected. Figure 6 (b) illustrates how pH affects the adsorption of Cr (VI) ions onto the Po- and An-biochar adsorbents. The adsorption of Cr(VI) ions was superior at acidic pH as opposed to basic pH, as shown in Figure 6(b). The ability of the Po-Biochar adsorbent to remove Cr(VI) ions dropped steadily from 10% to 80% when the pH rose from 2.0 to 10. The adsorption of Cr(VI) ions onto the produced An-Biochar adsorbents is depicted in Figure 6(b). The removal effectiveness diminished with increasing pH but was greater at an acidic pH of 2.0. The protonation of the modified charcoal adsorbent is sufficiently weak to provide electrostatic repulsion between the negatively charged ions and the surface of the produced adsorbent at pH values greater than 6.0. The primary form for removing Cr(VI) ions from the aqueous solution is $HCrO_2^-$, which is more prevalent at low pH values between 2.0 and 6.0. Accordingly, the clearance efficiency was better at lower pH values than at higher pH values. Therefore, at a pH of 2.0, the An-Biochar adsorbents showed the highest removal efficiency of Cr(VI) ions. Thus, a pH of 2.0 was used during the investigation.

3.3.3. Effect of the adsorbent dosage

The sorbent dose is another important parameter because it addresses the adsorbent–adsorbate interaction and illustrates the system's equilibrium. Figure 6 (c) shows the percentages of Cr(VI) ions removed in response to varying adsorbent dosages ranging from 1 to 3.0 g L^{-1}. The figure illustrates how increasing the biochar dose improved the removal efficiency of Cr(VI) ions. Because more binding sites are available for pollutant adsorption, removal effectiveness increases with increasing adsorbent dosage. However, both pollutants achieved the saturation point at a specific dosage of 3 g L^{-1}). Thus, the optimum removal efficiency of Cr(VI) was obtained at 3.0 g L^{-1} of the adsorbents, reaching 87.2% for An-biochar and 82.5% for Po-biochar, with corresponding experimental adsorption capacities (qe, exp) of 21.5 mg g^{-1} and 22.8 mg g^{-1}, respectively.

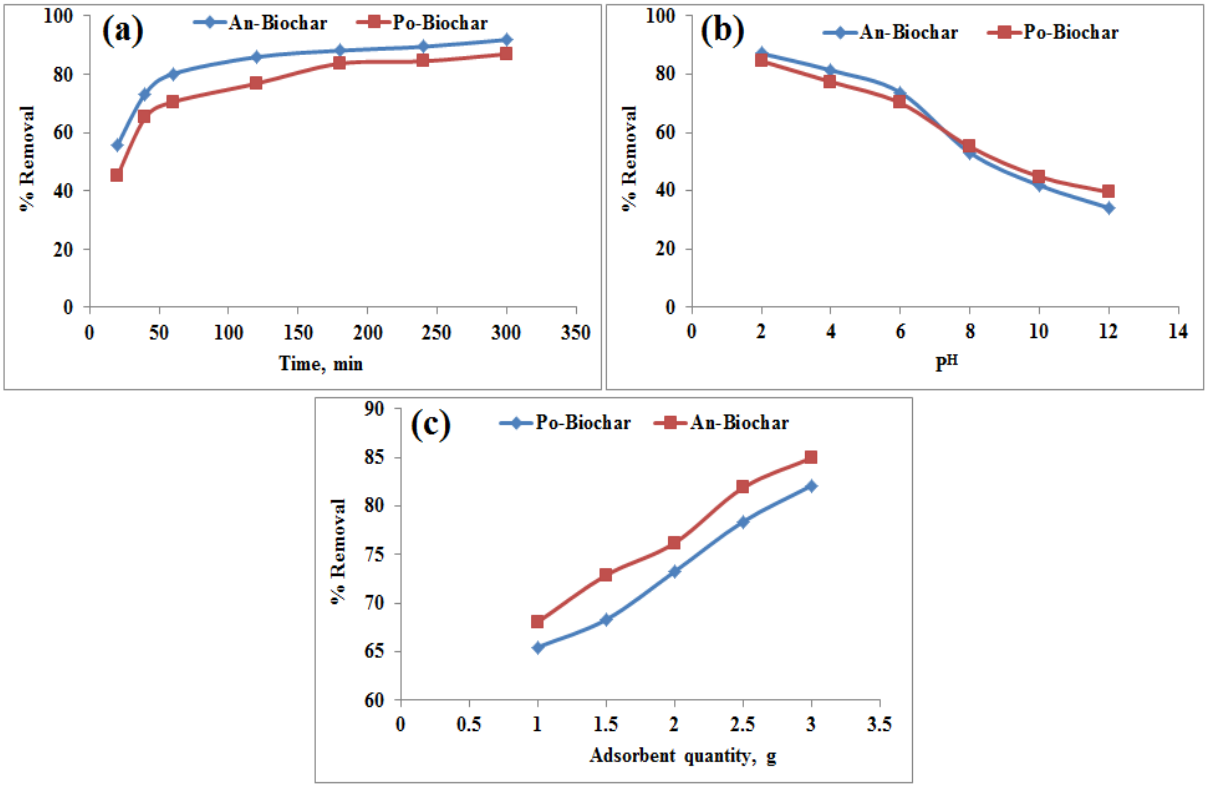

Figure 6. Adsorption study factors: **(a)** contact time, (b) pH, and (c) adsorbent dosage

3.4. Adsorption isotherms and kinetics of adsorption

3.4.1. Adsorption kinetics

The gathered data were fitted to pseudo-first-order and pseudo-second-order models to investigate the kinetic processes. Table 1 and Figure 7 show the kinetic models, their linear forms in equations (4) and (5), and the plot types employed to determine the kinetic parameters of each model. Here, qe (mg g^{-1}) is the adsorption capacity at equilibrium, qt (mg g^{-1}) is the quantity of Cr(VI) ions adsorbed after time t (min), and k_1 is the pseudo-first-order rate constant (min^{-1}). Pseudo-second-order model, where qe (mg g^{-1}) is the adsorption capacity at equilibrium, qt (mg g^{-1}) is the quantity of Cr(VI) ions adsorbed after time t (min), and k_2 is the pseudo-second-order rate constant (g $mg^{-1}min^{-1}$).

Table 1. Physical characteristics of Po- and An-Biochars

Sample	Model	Linearized equation	k	$qe_{(cal)}$ (mg/g)	$qe_{(exp)}$ (mg/g)	R^2
Po-Biochar	PFO	$\ln(qe\_-qt) = \ln qe\_-k_1t$ (4)	k_1=0.0540 min^{-1}	16.59	22.8	0.7646
Po-Biochar	PSO	$t/qt = 1/k_2qe^2 + t/qe$ (5)	k_2=0.000782 g mg^{-1} min^{-1}	23.42	22.8	0.8939
An-Biochar	PFO	$\ln(qe\_-qt) = \ln qe\_-k_1t$ (4)	k_1=0.0509 min^{-1}	12.69	21.5	0.8099
An-Biochar	PSO	$t/qt = 1/k_2qe^2 + t/qe$ (5)	k_2=0.001037 g mg^{-1} min^{-1}	22.03	21.5	0.9550

Table 1 presents the calculated kinetic parameters for Cr(VI) adsorption onto Po- and An-biochar. The pseudo-second-order model exhibited higher correlation coefficients (R^2 = 0.8939 and 0.9550) than those of the pseudo-first-order model (R^2 = 0.7646 and 0.8099). In addition, the calculated equilibrium adsorption capacities (qe_{cal}) obtained from the pseudo-second-order model were closer to the experimental values than those obtained from the pseudo-first-order model. These findings indicate that the pseudo-second-order model can better describe the adsorption kinetics, demonstrating that chemisorption is likely the rate-controlling mechanism in the adsorption process.

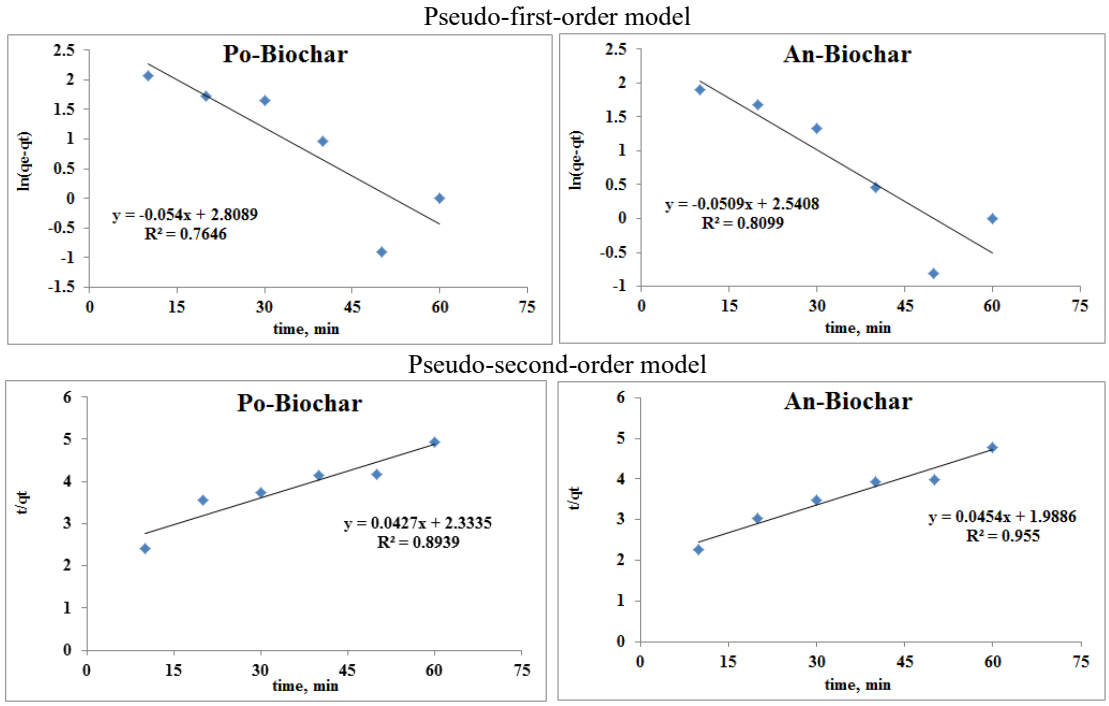

Figure 7.Pseudo-second-order and pseudo-first-order plots for Cr(VI) ions on Po- and An-biochars

3.5. Adsorption isotherm

Two-parameter (Langmuir and Freundlich) isotherm models were employed as adsorption isotherm models (Figure 8). The following linear forms of each model were employed in the adsorption isotherm models [15]:

$$Ce / qe = (Ce/qe) + 1/K_L*qm \quad [6] \text{ Linear Langmuir}$$

$$Log (qe) = Log K_F + 1/n \ \ Log Ce \quad (7) \text{ Linear Freundlich}$$

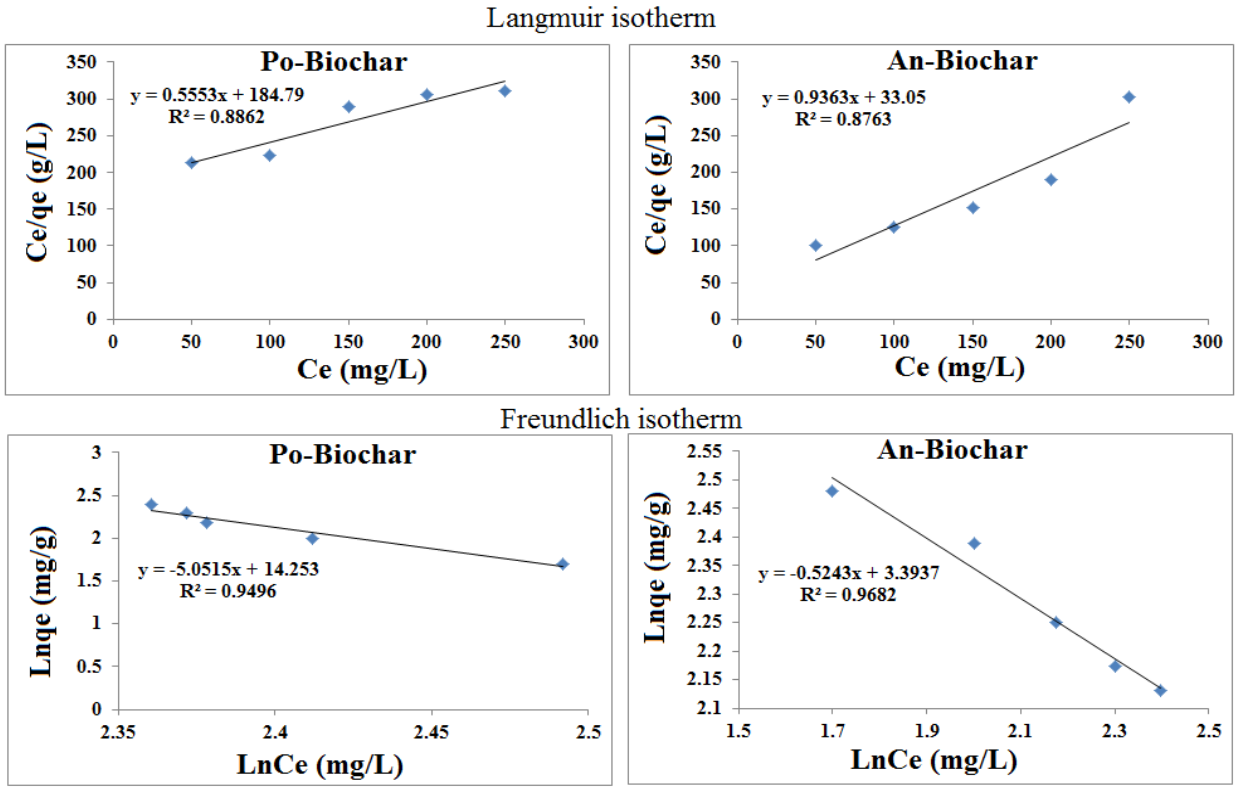

Figure 8. Langmuir and Freundlich isotherm model of Cr(VI) removal by Po- and An-biochar solvents at 298K

4. Conclusion

This study successfully demonstrated the synthesis of biochar via slow pyrolysis at 700 °C using two distinct local biomass feedstocks: pomegranate husks (Po-Biochar) and animal waste (An-Biochar). Textural characterization revealed that both materials possess a mesoporous structure; however, An-Biochar exhibited a higher BET specific surface area (63.81 m^2g^{-1}) and a larger average pore diameter (26.38 nm) than Po-Biochar (49.58 m^2g^{-1} and 17.52 nm, respectively), which correlates perfectly with the prominent hollow micro-sized structures observed in its FE-SEM morphology. The adsorption performance of hexavalent chromium Cr(VI) ions was found to be strongly pH-dependent, with both adsorbents achieving optimum removal efficiency under an acidic condition of pH 2.0 due to the prevalence of the $HCrO_4^-$ species and favorable electrostatic attraction on the protonated surfaces. Kinetic modeling indicated that the adsorption processes follow the pseudo-second-order model (R^2 = 0.9550 for An-Biochar and 0.8939 for Po-Biochar), where the calculated equilibrium adsorption capacities (qe, cal) of 22.03 mg g^{-1} for An-Biochar and 23.42 mg $g^{-1}$for Po-Biochar were in excellent agreement with the experimental values (qe, exp), confirming chemisorption as the rate-controlling mechanism. Furthermore, the Freundlich model fitted the equilibrium isotherm data significantly better than the Langmuir model, proving that a multi-layer adsorption process occurs over heterogeneous surface binding sites. Under optimum operating parameters (initial concentration of 50 mg L^{-1} and adsorbent dosage of 3.0 g L^{-1}), An-Biochar demonstrated a superior overall performance over Po-Biochar by achieving a maximum removal efficiency of 87.2% compared to 82.5% for Po-Biochar, highlighting its potential as a highly effective and ecologically sustainable bio-adsorbent.

Acknowledgment

I would like to thank the staff of Ba'aqubah Hospital in Diyala University for their cooperation and help during data collection. I am also very grateful to the willing research participants for this study. I would also like to thank all those who directly or indirectly helped me to complete this study.

References

[1] E. Kingsley et al., "Effect of hexavalent chromium on the environment and removal techniques: A review," J. Environ. Manage., vol. 280, p. 111809, 2021, doi: 10.1016/j.jenvman.2020.111809.
[2] S. Pooja, P. Surendra, K. Sheetal, and W. Yen, "Health hazards of hexavalent chromium (Cr (VI)) and its microbial reduction," Bioengineered, vol. 13, no. 3, pp. 4923–4938, 2022, doi: 10.1080/21655979.2022.2037273.
[3] S. Ewa, J. Karolina, and P. Agnieszka, "Chromium (III) and chromium (VI) as important players in the induction of genotoxicity – current view," Ann. Agric. Environ. Med., vol. 28, no. 1, pp. 1-10, 2021, doi: 10.26444/aaem/118228.
[4] K. Aisha et al., "Hydrochar as a bio-based adsorbent for heavy metals removal: A review of production processes, adsorption mechanisms, kinetic models, regeneration and reusability," Sci. Total Environ., vol. 945, p. 173972, 2024, doi: 10.1016/j.scitotenv.2024.173972.
[5] A. Jose, F. Jose, C. Leonidas, R. Igor, and S. Teogenes, "Influence of pyrolysis temperature and feedstock on the properties of biochars produced from agricultural and industrial wastes," J. Anal. Appl. Pyrolysis, vol. 149, p. 104839, 2020, doi: 10.1016/j.jaap.2020.104839.
[6] A. Reyhanitabar, E. Farhadi, H. Ramezanzadeh, and S. Oustan, "Effect of pyrolysis temperature and feedstock sources on physicochemical characteristics of biochar," J. Agric. Sci. Technol., vol. 22, no. 2, pp. 547-561, 2020. doi:10.22092/ijsr.2021.353431.582.
[7] S. Saroop et al., "Analyzing the impacts of three types of biochar on soil carbon fractions and physiochemical properties in a corn-soybean rotation," Chemosphere, vol. 184, pp. 473-481, 2017, doi: 10.1016/j.chemosphere.2017.05.165.
[8] M. Yichuan, Z. Shuting, and W. Jianlong, "Adsorption of heavy metals by biochar in aqueous solution: A review," Sci. Total Environ., vol. 968, p. 178898, 2025, doi: 10.1016/j.scitotenv.2025.178898.
[9] W. Yizhuo, L. He, and L. Shaohua, "Advances in the study of heavy metal adsorption from water and soil by modified biochar," Water, vol. 14, no. 23, p. 3894, 2022, doi: 10.3390/w14233894.
[10] V. Maria, J. Joan, V. Mariano, C. Eva, D. Belen, and J. Francisco, "Influence of feedstock and final pyrolysis temperature on breaking strength and dust production of wood-derived biochars," Sustainability, vol. 13, no. 21, p. 11871, 2021, doi: 10.3390/su132111871.
[11] Y. Ahmed et al., "Effect of pyrolysis temperature on biochar microstructural evolution, physicochemical characteristics, and its influence on biochar/polypropylene composites," Appl. Sci., vol. 9, no. 6, p. 1149, 2019, doi: 10.3390/app9061149.
[12] R. Narzari, N. Bordoloi, B. Sarma, L. Gogoi, N. Gogoi, and B. Borkotoki, "Fabrication of biochars obtained from the valorization of biowaste and evaluation of its physicochemical properties," Bioresour. Technol., vol. 242, pp. 324–328, 2017, doi: 10.1016/j.biortech.2017.04.050.
[13] L. Yongliang, H. Zhongqi, and U. Minori, "Comparison of biochar formation from various agricultural by-products using FTIR spectroscopy," Mod. Appl. Sci., vol. 9, no. 4, 2015, doi: 10.5539/mas.v9n4p246.
[14] M. Muhajir, C. Yonas, and T. Beteley, "Kinetics, adsorption isotherms, thermodynamics, and desorption studies of cadmium removal from aqueous solutions using bamboo sawdust/rice husk biochar," Biomass Convers. Biorefin., 2022, doi: 10.1007/s13399-022-03472-3.
[15] T. Prasetyo et al., "Adsorption isotherm model of Hg2+ with biochar from young coconut waste," IOP Conf. Ser.: Earth Environ. Sci., vol. 1297, p. 012093, 2024, doi: 10.1088/1755-1315/1297/1/012093.

BIOGRAPHIES OF THE AUTHORS

Safa A.Yassin holds a master's degree in physical chemistry and is a lecturer in the general direction for Diyala education.
safaahmed072@gmail.com